Development of flexible nanoporous gold electrodes for the detection of glucose

Denise Demurtas, Julia Alvarez-Malmagro, Arvind Rathore, Tanushree Mandal, Andrés Felipe Quintero-Jaime, Serguei Belochapkine, Anna Lielpetere, Kavita Jayakumar, Dónal Leech, Wolfgang Schuhmann, et al.

Bioelectrochemistry 165 (2025) 108949

Contents lists available at ScienceDirect

Bioelectrochemistry

journal homepage: www.journals.elsevier.com/bioelectrochemistry

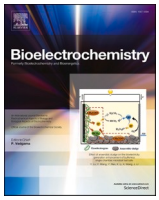

Development of flexible nanoporous gold electrodes for the detection of glucose

Denise Demurtas [a], Julia Alvarez-Malmagro [a], Arvind Rathore [b], Tanushree Mandal [c], Andrés Felipe Quintero-Jaime [a], Serguei Belochapkine [a], Anna Lielpetere [d], Kavita Jayakumar [c], Dónal Leech [c], Wolfgang Schuhmann [d], Nicolas Mano [e], Claudine Boiziau [b], Edmond Magner [a,*]

[a] Department of Chemical Sciences, Bernal Institute University of Limerick V94 T9PX, Limerick, Ireland
[b] Univ. Bordeaux, INSERM, BioTis, U1026, F-33 000 Bordeaux, France
[c] School of Chemistry & Ryan Institute, University of Galway, University Road, Galway, Ireland
[d] Analytical Chemistry - Center for Electrochemical Sciences, Faculty of Chemistry and Biochemistry, Ruhr-University Bochum, 44780 Bochum, Germany
[e] Centre de Recherche Paul Pascal (CRPP) CNRS UMR 5031 Univ, Bordeaux 115 Avenue du Docteur Schweitzer, 33600 Pessac, France

ARTICLE INFO

Keywords:
Nanoporous gold
Glucose monitoring
Implantable electrodes, foreign body reaction

ABSTRACT

The development of implantable glucose sensors is of significant interest in the management of diabetes. This work focuses on developing an implantable, biocompatible nanoporous gold electrode prototype based on Kapton® for the subcutaneous detection of glucose. The electrodes were first modified with a layer containing glucose oxidase and Os(2,2′-bipyridine)$_2$Cl·PVI (Os(bpy)$_2$Cl PVI). An additional polymeric layer containing poly (2-methacryloyloxyethyl phosphorylcholine-co-glycidyl methacrylate) was then added to reduce biofouling and foreign body reaction effects. The modified electrode had a V_{MAX} of 211 ± 13 μA cm^{-2} and a K_{Mapp} of 6.1 ± 0.8 mM in pseudo physiological conditions, with a linear detection range from 1 to 4 mM and a sensitivity of 28.6 ± 2.1 μA cm^{-2} mM^{-1}. In artificial plasma, the response of the sensor was saturated at 3 mM, with a V_{MAX} of 113 ± 10 μA cm^{-2} and a K_{Mapp} of 2.1 ± 0.4 mM with a linear detection range from 1 to 2.5 mM and a sensitivity of 14.6 ± 3.3 μA cm^{-2} mM^{-1}. Mechanical stress testing demonstrated that there was a 40 % reduction of the redox polymer coverage after 320 deformation events, however the catalytic activity was still detectable after 160 events. Minimal cytotoxicity effects of the electrodes were observed. When subcutaneously implanted the electrodes showed fairly good mechanical stability after one week and detachment of the metallic layer on some electrodes after 21 days, probably due to electrode bending. A limited foreign body reaction was observed. These results indicated that the electrodes could be implanted for a period of up to 1 week.

1. Introduction

Continuous glucose monitoring in real-time is essential for managing diabetes as it can prevent complications caused by hyper- and hypoglycaemic episodes [1], significantly improving patients' quality of life. Electrochemical enzymatic sensors are effective technology for monitoring the glucose concentration in blood because of their sensitivity and specificity [2], rapid response, portability, accuracy, ease of use and cost-effectiveness [3].

Multiple approaches and methodologies for glucose detection have been developed, and they can be invasive, minimally invasive and non-invasive [4]. Depending on the diagnostic goal, some are preferred to others, i.e. finger-prick monitoring is accurate but reduces the patient's quality of life [5] on the contrary wearable biosensors are highly comfortable but may be inaccurate due to the poor correlation between glucose in blood and in sweat [6]. Implantation of glucose sensors is required when high accuracy and long-term monitoring are needed [7]. Of particular interest is the design of implants based on supports that match the mechanical properties of the target tissue, and that are biocompatible with minimal inflammatory response [8]. The need for supports to endure mechanical stress while enabling signal transduction has led to a more holistic approach in the design of tissue-like bioelectronics [8], where the mechanical, chemical and biological properties of tissue are taken into account [9]. Modification of flexible substrates to produce flexible electrochemical systems has been widely investigated with carbon materials [10] and nanostructured metals

* Corresponding author.
E-mail address: edmond.magner@ul.ie (E. Magner).

https://doi.org/10.1016/j.bioelechem.2025.108949
Received 1 November 2024; Received in revised form 23 January 2025; Accepted 22 February 2025
Available online 24 February 2025

[11]. Carbon materials provide excellent electrochemical performance due to their high surface areas [12] and compatibility with enzymes. However, they can be mechanically fragile, requiring mechanical support [13] when implanted, and some carbon nanomaterials may display cytotoxic effects [14]. Nanoporous gold electrodes (NPGs) can avoid these drawbacks since they can be prepared on mechanically stable supports [11], and Au is a well-established biocompatible material.

When devices are implanted in biological systems, the sample matrix can significantly affect the performance of the device. The majority of sensors used for diabetes management are electrochemical and rely on a glucose-oxidising enzyme and determine the concentration of glucose in the tissue using amperometry [15]. These devices operate in many configurations, they can indirectly detect a reaction product through its oxidation or reduction at the electrode (i.e. hydrogen peroxide); allow the detection of an electrons flux from the enzyme employing a mediator (mediated electron transfer MET) or directly from the enzyme (direct electron transfer DET) [3,16]. Tests under laboratory conditions can only simulate biological conditions containing a range of species, such as ascorbic acid (AA) and uric acid (UA), or protein content that can hinder the performance of enzyme-based electrochemical systems, i.e. bovine serum albumin (BSA). Uric acid, for example, acts as a noncompetitive inhibitor of some glucose oxidising enzymes, e.g. glucose dehydrogenase (GDH), glucose oxidase (GOx), and cellobiose dehydrogenase (CDH) [17] which explains worsened current outputs in artificial plasma. BSA is a common protein used to simulate biofouling it has been proven not to affect NPG electrodes performance when tested at physiological concentrations [11].

The implantation of devices triggers inflammatory responses, initially by the wound caused by the surgical procedure and subsequently by the reaction of the immune system and the surrounding tissues to the implanted material, perceived as a foreign body, promoting what is known as the foreign body reaction (FBR) [18]. The degree of FBR depends on the implantation site and the device characteristics (such as size, stiffness, surface-chemical and -physical properties). Kapton® is a suitable material as it possesses good mechanical and chemical stability, can withstand common sterilisation procedures such as gamma irradiation [19] and, most importantly, possesses good biocompatibility when coated [20]. The general inflammatory process occurs in the following described steps [21]. In the initial phase, a range of species adsorb on the surface, including proteins. During the first 24 h, neutrophils and mast cells are recruited and activated in the vicinity of the device, releasing proteases and reactive oxygen species (ROS) such as hydrogen peroxide and superoxide, cytokines and growth factors that contribute to the recruitment of other cells (monocytes, lymphocytes). The monocytes differentiate into macrophages with pro-inflammatory properties with the goal of degrading the foreign body. In the presence of non-biodegradable materials such as those used for glucose biosensors, macrophages activate myofibroblasts and blood-born fibrocytes that produce a collagenous extracellular matrix that isolates the material from the surrounding tissues [21]. Limiting the FBR formation is of importance for electrochemical devices based on diffusion of the analytes from the surrounding tissue because it hinders it, increasing the time needed for a reliable measurement [22]. Many strategies have been explored to limit FBR, including surface coating [23]. Zwitterionic polymers have been shown to improve FBR such as methacryloyloxyethyl phosphorylcholine (MPC) [24], and carboxy- [25] and sulfo- [26] betaine showing thinner FBR capsule formation; attributable both to their chemistry that improves the hydration sphere around the electrodes, as well as their low Young modulus as the final coating layer.

In this work, NPG electrodes were prepared using Kapton® as a biocompatible and mechanically stable support. The anode was comprised of glucose oxidase from *Aspergillus niger* (GOx) and an Os-complex modified polymer [Os(2,2 bipyridine)$_2$ (poly-vinylimidazole)$_{10}$ Cl]$^+$, coated with an anti-biofouling layer of poly(2-methacryloyloxyethyl phosphorylcholine-*co*-glycidyl methacrylate (MPC). The electrode properties were thoroughly characterized and demonstrated promising mechanical stress resistance in vitro and in vivo, with no evident cytotoxicity and acceptable biocompatibility.

2. Experimental

2.1. Reagents and solutions

The following reagents were purchased from Sigma-Aldrich, poly (ethylene glycol) diglycidyl ether Mn 500 (PEDGE-500), uric acid (UA, ≥ 99 %), L-ascorbic acid (AA, ≥ 99 %), D-glucose (Glu, ACS reagent), D-fructose (≥ 99 %), D-lactose (≥ 99 %), urea (ACS reagent), l-cystine (≥ 99.7 %) (0.075 mM), NaH_2PO_4 (≥ 99 %), Na_2HPO_4 (≥ 99 %), calcium sulphate dehydrate (ACS reagent, 98 %), magnesium sulphate (≥ 99.5 %), sodium chloride (≥ 99), sodium bicarbonate (ACS reagent), nitric acid (ACS grade 70 %), sulfuric acid (95–98 %), Neutral Red assay, MTT (3-(4, 5-dimethylthiazolyl-2)-2, 5-diphenyltetrazolium bromide) assay, bovine serum albumin (BSA) (≥ 96 %), Triton X-100 and absolute ethanol. Kapton® 50 HN sheets (50 μm thick) were obtained from Dupont. The cell culture medium was minimum essential medium α (α-MEM, Gibco, France), implemented with 10 % (*v*/v) fetal calf serum, (FCS), Lonza, France.

Glucose oxidase from *Aspergillus niger* (GOx, EC 1.1.3.4, type X-S, 100–250 kU g^{-1}) was purchased from Sigma Aldrich. Milli-Q® water (Milli-Q®) with a resistivity of 18.2 MΩ cm was generated by an Elgastat Purelab Pulse system (Elga, UK) and used to prepare all aqueous solutions. The osmium redox polymer [Os(2,2 bipyridine)$_2$ (poly-vinylimidazole)$_{10}$ Cl]$^+$, denoted as (Os(bpy)$_2$Cl PVI) was synthesised as described by Mercer et al. [27] with a formal redox potential of +250 mV vs Ag/AgCl 3 M KCl extracted from cyclic voltammetry (CV). Poly(2-methacryloyloxyethyl phosphorylcholine-*co*-glycidyl methacrylate (MPC) was synthesised as reported previously [28]. Tissue samples preparation for histological analysis was performed by using 4 % para-formaldehyde in phosphate buffer saline (PBS) (AntigenFix, Diapath, Martinengo, Italy) and embedded in optimal cutting temperature tissue freezing medium (OCT TFM-C, MM France, Brignais, France).

2.2. Electrode preparation

Nanoporous gold electrodes (NPGs) were prepared using Kapton® as substrate employing magnetron sputtering in an ultra-high vacuum chamber (ORION-5-UHV) at room temperature (RT), 21 °C, equipped with 3 metal targets (99.99 % purity), Au, Ag and Ti (Kurt J. Lesker Company Ltd.,UK) for substrate deposition. A 10 nm Ti adhesion layer was deposited, followed by an Au layer with one-third of the thickness of the subsequent layer of alloy. A Ag_{30}/Au_{70} alloy layer (100 nm) was deposited on top of this layer. Prior to metal deposition, the Kapton® HN sheets were exposed to Ar/O_2 plasma (1:1) 20 W for 1 min under vacuum to ensure a clean surface and improve adhesion and homogeneous deposition of the metal [29].

In order to obtain different pore sizes in the NPG electrodes, portions of the modified Kapton® sheets were cut and dealloyed by corrosion of Ag from the alloy layer in 70 % nitric acid at different conditions: at 20 °C for 1 and 5 min and at 40 °C for 5 min. The electrodes dealloyed at 40 °C for 5 min were employed in the mechanical resistance test and implantation. After the formation of the nanopores, the electrodes were rinsed and sonicated for 10 min with Milli-Q®. Finally, they were dried in a vacuum chamber for at least one hour. Once the surface was dry, a silver wire (Farnell Components Ltd. Ireland) was connected using a conductive carbon-based glue (Loctite® EDAG PF 407 A E&C) or soldered to the surface using an indium (99.999 % purity) wire (Sigma–Aldrich Ltd.). The connection point was supported by a two-component epoxy glue (Araldite) to increase the mechanical resistance of the anodes for the implantation. Dielectric paste (Gwent Group, UK) was used to insulate the electrode components and to protect the Kapton® from water permeation, resulting in a geometrical surface area of 0.25 ± 0.05

cm^2.

2.3. Mechanical resistance evaluation in vitro

NPG electrodes were exposed to mechanical stress using a 3D-printed device (Fig. 1) to bend the electrodes at an angle of 20° on each side. Mechanical stress was applied alternatively to the gold electroactive NPG surface and the dielectric coated Kapton® side (insulating portion), for a total of 320 bending events (16 deformation cycles corresponding to 20 bending events each). The device was anchored to the bench via its base. A final bending angle of 180° was applied to verify the flexibility of the nanoporous structure on the electrode. The variation of the electroactive surface area (ECSA) and the stability of the connection were measured using CV.

2.4. Electrode modification

NPG electrodes (12) with surface areas of ca.0.25 cm^2 dealloyed at 40 °C for 5 min were modified with $Os(bpy)_2Cl$ PVI (150 μg), GOx (160 μg), and PEDGE (34 μg). These aqueous solutions were mixed directly onto the electrode surface using a micropipette. After allowing the active layer to dry for 1 h in a vacuum chamber at RT, an aliquot of MPC polymer (100 μg) was allowed to dry overnight at 21 °C previous measurement (Fig. 2).

2.5. Electrochemical measurements

Electrochemical studies were performed using a CHI1030 potentiostat (CH Instruments, Austin, Texas). A standard three-electrode cell configuration was used for the characterisation of the electrodes, with a modified NPG as a work electrode (WE), a platinum mesh (ALS Co. Ltd., Tokyo, Japan) as the counter electrode (CE) and a Ag/AgCl/3 M KCl (IJ Cambria Scientific Ltd., UK) as the reference electrode (RE).

The electroactive surface area (ECSA) was determined through electrochemical stripping of gold oxide by applying a potential scan from −0.2 to 1.65 V vs Ag/AgCl at 0.1 Vs^{-1} in 0.5 M H_2SO_4. The charge associated with the gold oxide peak was used to measure the surface area using a conversion factor of 390μC cm^{-2} [30]. The geometric surface area (A_{geo}) was determined by taking a high-resolution micrograph of each NPG electrode on a millimetre grid, followed by analysis with ImageJ software [31].

The properties of the electrodes were examined in 50 mM phosphate buffer solutions containing 150 mM NaCl at pH 7.4 (PBS) or in artificial plasma (AP) prepared as previously described [32]; at RT, unless specified otherwise. An aqueous stock solution of glucose (2 M) was prepared and allowed to come to equilibrium for 24 h before any measurements and kept overnight at RT. After conditioning for 30 min in 0.05 M phosphate, 0.15 M NaCl, pH 7.4 or AP, the response of the bioanode was examined using amperometry (E = 0.4 V vs Ag/AgCl with stirring at 150 rpm) or cyclic voltammetry over the potential range 0.05–0.4 V vs Ag/AgCl. The sensitivity was determined by applying a linear regression model to the linear region of the calibration curve to determine the slope. The kinetics parameters (V_{max} and $K_{M\ app}$) were determined (eq. S1) using a non linear regression model to the data points. The limit of detection (LOD) and limit of quantification (LOQ) were determined using eqs. S2 and S3. The coverage of Os complex (Γ) was estimated from the peak charges obtained using cyclic voltammetry at a slow scan rate (1):

$$\Gamma = \frac{Q}{nFA_{geo}} \quad (1)$$

where Q is the charge of the oxidative peak, n is the number of electrons exchanged in the redox process, F is Faraday's constant and A_{geo} is the geometric area in cm^2 [33].

2.6. Cytotoxicity

Unmodified and functionalised NPG electrodes with the Os complex $Os(bpy)_2Cl$ PVI (5 mg mL^{-1}, 30 μL), GOx (10 mg ml^{-1}, 30 μL) and cross-linker PEGDGE (Mn 500) were tested for cytotoxicity. This was assessed according to the international standard ISO10993-5. Extracts were prepared according to ISO 10993-12 by incubating the devices in the culture medium (6 cm^2 mL^{-1}) at 37 °C for 24 h, providing the "Day 1" extract. New medium was added to the electrodes for a second and a third incubation of 24 h at 37 °C ("Day 2" and "Day 3" extracts). The extracts were subsequently supplemented with 10 % (*v*/v) fetal calf serum; a 100 μL aliquot was added to the cell line (L929), previously seeded at 10.000 cells cm^{-2} in 96-well plates (Nunc, Denmark) and cultured for 72 h.

Wells containing only the medium were used as a reference as a negative control, providing the 100 % value of survival (C), while positive controls (PC) of toxicity were performed in parallel, adding Triton X-100 0.1 % (v/v) in the culture medium. Culture plates were left at 37 °C in 5 % CO_2 for 24 h. After incubation, cell viability was assessed using a Neutral Red assay and cell metabolic activity by an MTT assay [34]. The mean survival and metabolism measurement values obtained from colorimetric tests were calculated from six repeats for each electrode. The results are presented in histograms as percentages of the reference "C" (alpha-MEM + 10 % FCS), with mean ± s.d. for 4 electrodes in each condition. A material is deemed to have no cytotoxic potential if the cell viability is over 70 % of the control value.

2.7. Mechanical resistance evaluation after implantation

The mechanical resistance of electrodes was assessed in vivo by implantation in rats. All animal studies were carried out in accredited animal facilities at the University of Bordeaux (accreditation number: A33–063-917), and the project received the authorisation of the French Ministry of Higher Education, Research and Education (APAFIS #16443–2,018,072,016,398,155 v4). The animals, 6 female Sprague Dawley rats (12–14 week-old, 250 g), were housed together in cages (3 rats per cage) in an enriched environment (houses and nesting) with a 12-h day/night cycle and food, and water ad libitum.

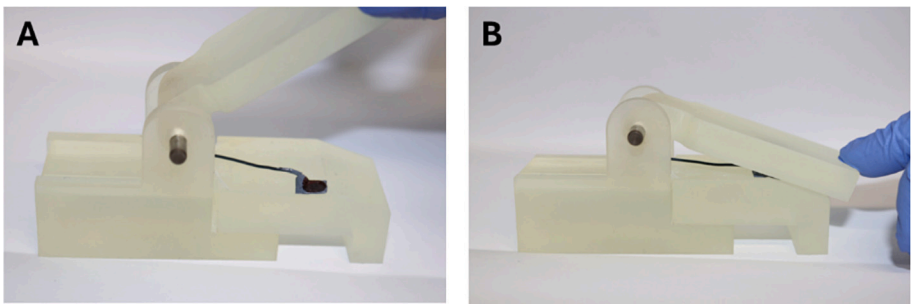

Fig. 1. Images of an electrode placed in the test device (A) before and (B) after application of mechanical stress.

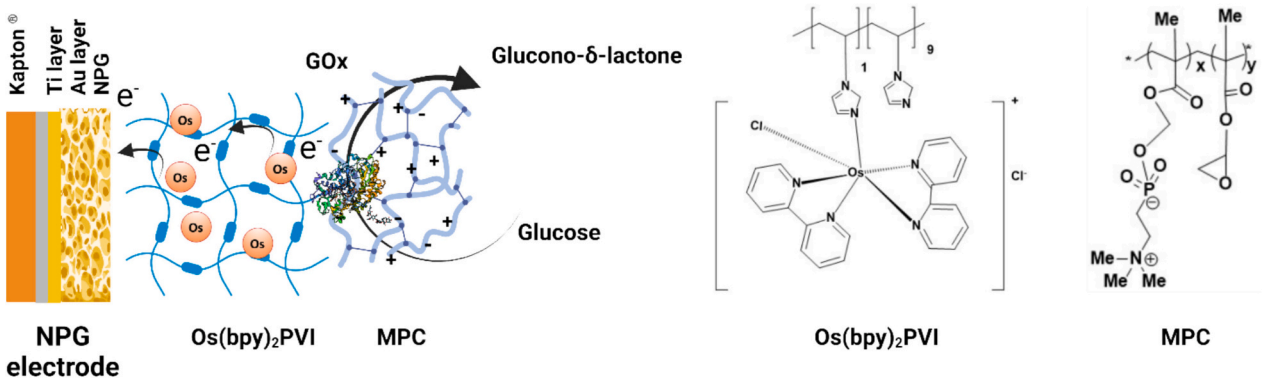

Fig. 2. Schematic representation of the modified anode (not to scale). Created in BioRender. Demurtas, D. (2025) https://BioRender.com/z38y847

The unmodified side and the wire were disinfected using 70 % ethanol. The electrodes were subcutaneously implanted on the shaved and disinfected back of the animal parallel to their spine and left for 7 or 21 days (2 electrodes/rat, 6 electrodes per time point). Electrode integrity was monitored by X-ray imaging (MX20-DC2 digital imaging instrument, Faxitron Bioptics, Arizona, USA), after euthanasia by CO_2 inhalation. Afterwards, the tissue containing the electrode was dissected, fixed for 3 days in 4 % paraformaldehyde (AntigenFix, Diapath, Martinengo, Italy), embedded in OCT (TFM-C, MM France, Brignais, France) and 10 μm thick sections were prepared on a Leica CM 3050S cryostat (Leica Microsystems, Wetzlar, Germany). Masson's trichrome staining was performed and imaged on a Nikon microscope (Eclipse 80i).

3. Results and discussion

3.1. Morphological analysis

NPG electrodes were prepared on a Kapton® support using the dealloying conditions described. SEM images (Fig. S1) show that exposure of the alloy to HNO_3 as a function of time and temperature influenced the characteristics of the porous structure [35]. The average pore size increased with increasing temperature and incubation time [36]. Electrodes dealloyed for 1 and 5 min at 20 °C had average pore sizes of 17 nm while dealloying at 40 °C for 5 min resulted in an average pore size of ca. 33 nm [36]; with roughness factors (R_f) of (16 ± 4) to (10 ± 8) and (6 ± 1) respectively that decreased with increasing exposure time and temperature (Table 1). NPG@Kapton® electrodes dealloyed at 40 °C for 5 min had smaller average pore diameters of ca. 10 nm when compared to electrodes prepared using glass substrates [35] while the R_f values were two-fold larger. The basis for the smaller pore sizes is unclear but may be related to the higher flexibility of the film on Kapton® supports. Electrodes dealloyed at 40 °C for 5 min were employed for mechanical resistance and implantation testing.

3.2. Impact of mechanical stress on electrochemical behaviour

Implantable devices must withstand the mechanical forces induced by the movement of the surrounding muscular tissue. The resistance to mechanical stress was examined using a custom-made device (Fig. 1), to simulate the bending that the electrodes will encounter after implantation below the cervical vertebrae and next to the thoracic vertebrae of the rats. Twisting and torsion were not considered due to the implant location of the implanted device. An angle of 20° was chosen to apply mechanical stress that was more demanding than the actual stress experienced on implantation where stress angles would be lower. The electrode response was examined in H_2SO_4 after repetitive deformation through cyclic voltammetry, indicated by the number of deformation events (Fig. 3 A). The change in ECSA was calculated after each deformation cycle (corresponding to 20 consecutive mechanical deformations on opposite sides of the electrodes, (Fig. 3 B).

Table 1
Average pore size and roughness factor (R_f) obtained at different dealloying conditions for NPG@Kapton®.

Dealloying Conditions	Average pore size [nm]	Roughness factor [R_f]	Residual Ag [wt %]
Pristine alloy	None	NA	70
20 °C, 1 min	17	16 ± 4	3.2
20 °C, 5 min	15	6 ± 1	Undetected
40 °C, 5 min	33	10 ± 8	Undetected

The electrodes showed no visible structural deformation or delamination when manually bent at 180° or during the stress application cycles, confirming their suitability for implantation. However, they showed a reduction of up to 50 % in ECSA after 320 repetitions (Fig. 3 B). Mechanical stress was alternatively applied to each side of the electrodes, resulting in a partial recovery of the ECSA obtained after applying stress on the Kapton® side. This behaviour can be attributed to the compression and relaxation of the pores that can occur when the electrode is bent on the NPG side and the Kapton® respectively, affecting the measured ECSA [37]. While a stronger support material could be used, for example using a thicker Kapton® layer this was deemed to not be necessary as the mechanical stress angle used was larger than what would occur on implantation.

After examining the impact of mechanical stress on bare NPGs, the performance of the redox hydrogel was examined. The coverage of the redox-active polymer in the absence of glucose (Fig. 4) decreased to 40 % after 320 mechanical stress events, in good agreement with the 50 % loss of ECSA observed on the bare electrodes ($n = 3$). The stability of the redox polymer decreased linearly until approximately 100 stress events, after which the coverage decreased to 40 %. This behaviour can be explained by the leaching of the redox moieties into the bulk solution, as previously described [38], an effect that may become more pronounced when bending the electrode. In addition, continuous potential cycling can cause counterion movement with shrinking and swelling of the polymer layer that can potentially affect its stability [39].

When the response of the electrode was examined in the presence of 10 mM glucose (Fig. 5) [40], the current increased initially after 140 repetitions (n = 3), an increase that may be ascribed to a more accessible enzyme layer (Fig. 5). After 260 repetitions (Fig. 5, black dashed line), an ohmic resistive response was obtained, that likely arises from (partial) breakage of the connection between the electrode and the wire. Higher resistance was observed arising from (partial) breakage of the connection between the electrode and the wire.

3.3. NPG@Kapton bioanodes

The modified electrodes were then electrochemically tested to verify

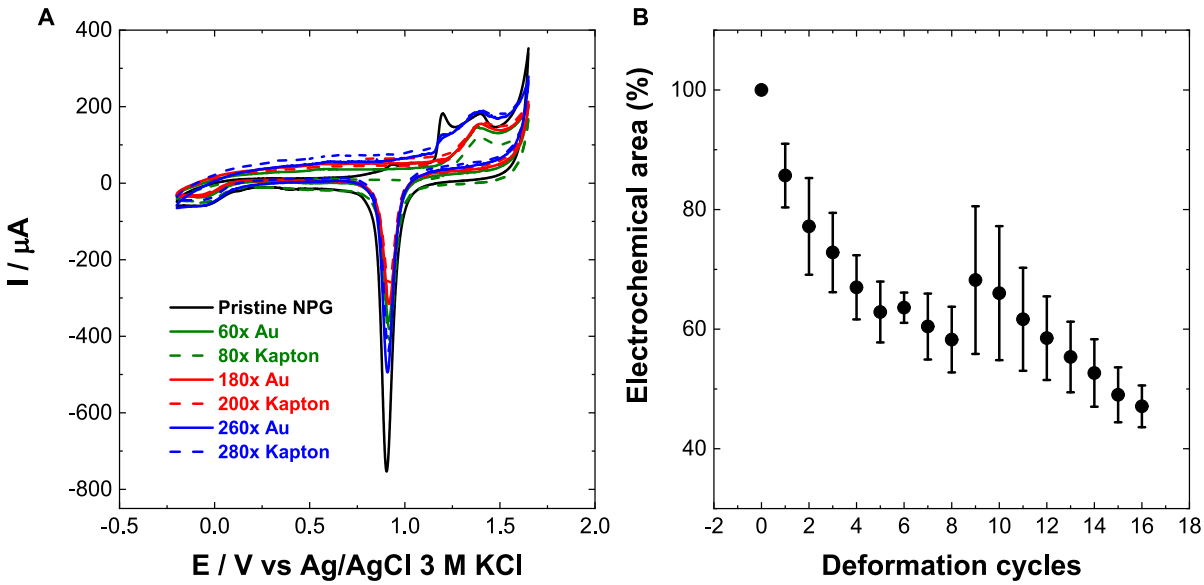

Fig. 3. (A) Cyclic voltammograms of the NPG electrode before and after deformation (B) Plot of electroactive area (%) before and after deformation. Measurement conditions: 50 mM H_2SO_4, scan rate 100 mV s^{-1} vs Ag/AgCl 3 M KCl.

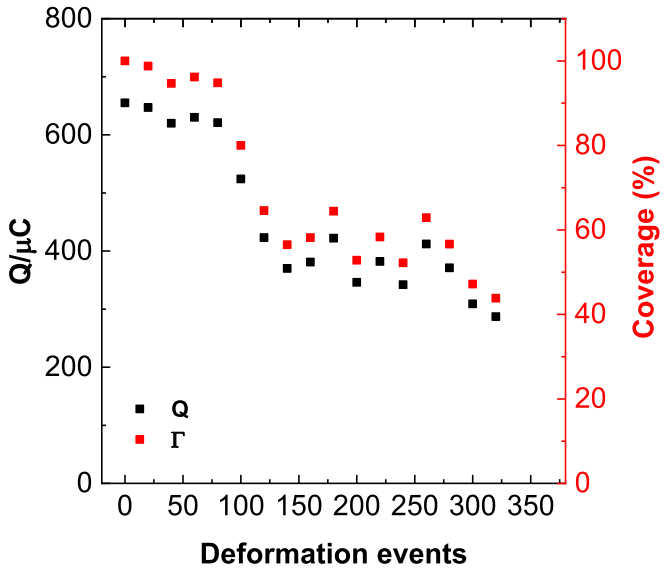

Fig. 4. Plots of the charge and coverage of the $Os(bpy)_2Cl$ PVI polymer as a function of mechanical bending. Measurement conditions: 0.05 M phosphate, 0.15 M NaCl, pH 7.4 at RT.

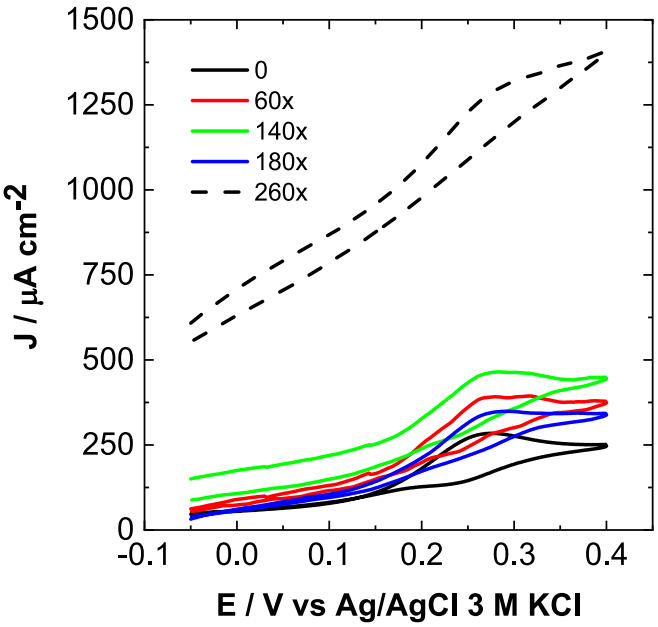

Fig. 5. Cyclic voltammograms of GOx/$Os(bpy)_2Cl$ PVI/PEDGE-500/NPG@Kapton® in PBS containing as a function of the number of deformations. Measurement conditions: scan rate 5 mV s^{-1} vs Ag/AgCl 3 M KCl at RT.

their functionality in phosphate buffer saline and artificial plasma. The anode showed the typical behaviour of catalytic activity in the substrate's presence, confirming the glucose oxidase's effective wiring and its successful electron transfer with an Os complex coverage of 4.6 pmol cm^{-2}. In vitro measurements in pseudo physiological conditions show a V_{MAX} of 210.8 ± 13.1 µA cm^{-2} and a K_{Mapp} of 6.1 ± 0.8 mM (Fig. 6 B and **Fig. S1** A) with a linear range of up to 4 mM and a sensitivity of 28.6 ± 2.1 µA cm^{-2} mM^{-1}. The values of V_{MAX} for GOx on NPG electrodes were significantly different than those previously reported as (4000 µA cm^{-2} and a $K_{M\ app}$ of 40.8 ± 5.5 mM [41]. The electrodes used previously had a smaller average pore diameter (between 12 and 20 nm) obtained on a gold leaf transferred to a glassy carbon electrode support; the calibration was obtained using cyclic voltammetry at the scan rate of 5 mV s^{-1}, which is a less sensitive technique compared to amperometric measurements [33]. Limits of detection (LOD) of 0.047 µM and quantification (LOQ) of 0.143 mM were obtained by using the calibration curve method based on the standard deviation of the blank Eq. 2 and 3 in the SI [41]. The decreased current at multilayered modified electrodes arises from hindered diffusion of glucose through the matrix. Further optimisation of the design to improve the linear range in these conditions is needed. While higher amounts of enzyme may lead to an increase in stability, this may come at the cost of additional diffusional limitations.

Amperometric calibration in artificial plasma, (Fig. 7 A and B), showed lower electrochemical performance compared to the one reported in phosphate buffer, reaching saturation at 3 mM and V_{MAX} of 112.7 ± 9.9 µA cm^{-2} and a K_{Mapp} of 2.1 ± 0.4 mM with linear ranges up to 2 and 2.5 mM and a sensitivity of 14.6 ± 3.3 µA cm^{-2} mM^{-1}. MPC-

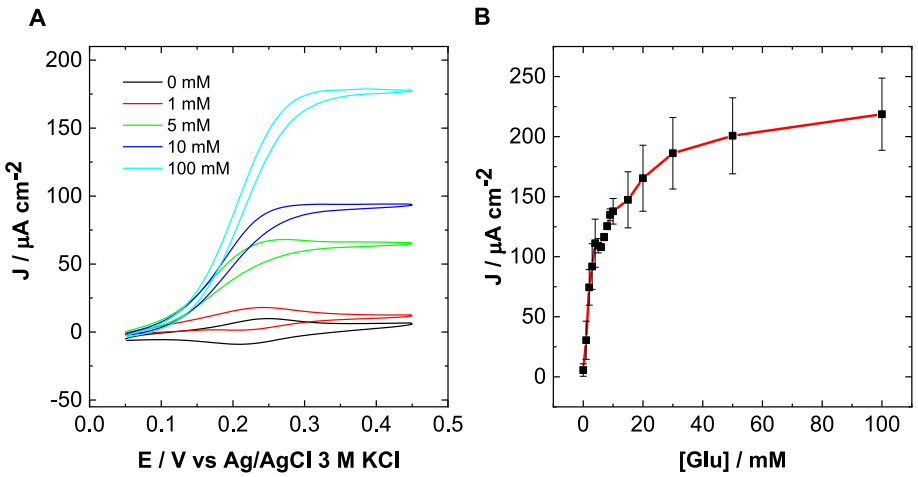

Fig. 6. (A) Cyclic voltammograms of the MPC/GOx/Os(bpy)$_2$Cl PVI/PEDGE-500/NPG@Kapton® in PBS in the presence of increasing glucose concentration. Measurement conditions: scan rate 1 mV s^{-1} vs Ag/AgCl 3 M KCl at 37.5 °C. (B) Baseline-corrected amperometric response as a function of glucose concentration, extracted from amperometry at 0.4 V vs Ag/AgCl/3 M KCl for electrodes (n = 3) under continuous stirring at 150 rpm.

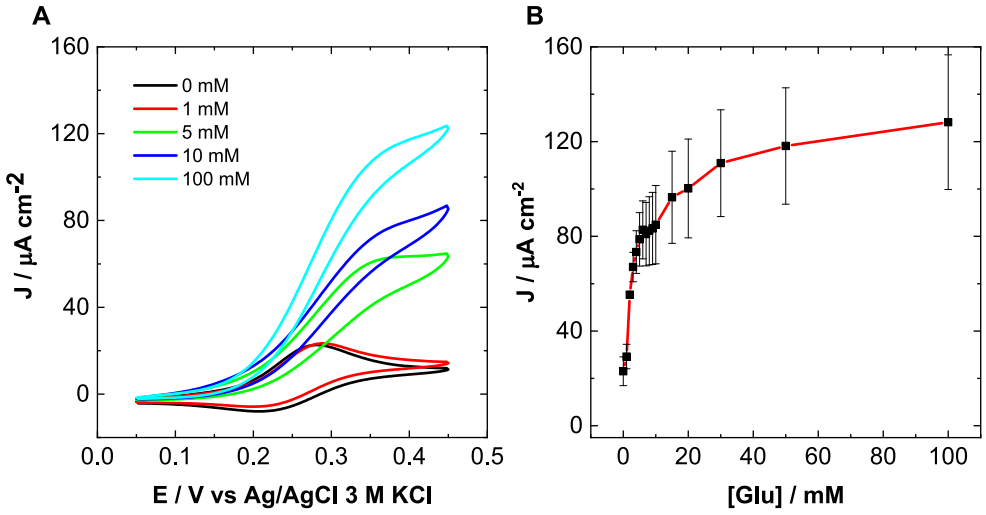

Fig. 7. (A) Cyclic voltammograms of the MPC/GOx/Os(bpy)$_2$Cl PVI/PEDGE-500/NPG@Kapton® in artificial plasma in the presence of increasing glucose concentration. Measurement conditions: scan rate 1 mV s^{-1} vs Ag/AgCl/3 M KCl at 37.5 °C. (B) Baseline corrected amperometric response as a function of glucose concentration, extracted from amperometry at 0.4 V vs Ag/AgCl/3 M KCl for electrodes (n = 3) under continuous stirring at 150 rpm.

coated electrodes, respectively. LOD and LOQ were calculated as 4.44 µM and 1.35 µM. While the lower response can be attributed to the increased viscosity which limits the diffusion of the species, the presence of inhibitors and partial biofouling of the electrodes, the sensor is still capable of detecting hyperglycaemia both in pseudo-physiological and artificial plasma.

3.4. Cytotoxicity

The cytotoxicity of the modified NPG electrodes on glass with Os(bpy)$_2$Cl PVI, GOx and PEDGE was tested before implantation. Indeed, it is recommended that medical devices be assessed for potential cytotoxicity prior to implantation in laboratory animals. To confirm that the NPG electrodes released no cytotoxic products, four unmodified electrodes and four others modified with the Os-complex-based polymer, GOx and the PEDGE cross-linker were incubated in the culture medium for 3 successive days. Extracts were taken each day to determine if any toxic products were released early (during the first 24 h in the medium) or later (during the second or third day). The survival and metabolism of immortalised murine fibroblasts L929 were compared when incubated in the presence of these extracts. The limit of toxicity defined by the standard method is 70 %. The positive control (PC) showed a high level of cytotoxicity (Fig. 8 A) while all extracts retained more than 70 % of the reference response for cell survival((Fig. 8 A) and cell metabolism (Fig. 8 B). These results indicated that it was feasible to proceed with in vivo implantation for the foreign body response analysis.

3.5. Mechanical resistance evaluation after implantation

Once it was demonstrated that the modified electrodes were not cytotoxic, 12 electrodes modified with Os-complex-based polymer, GOx and PEDGE coated with MPC layer were prepared and subcutaneously implanted in rats for 7 or 21 days. Our aim was to assess their mechanical stability when subjected to the movements of animals. The metal part of the electrodes could be visualised in rats before dissection by X-ray imaging (Fig. 9 A). This allowed us to show that 7 days after implantation, 5 out of 6 electrodes were still covered by the gold layer (the one that had lost the metal layer, implanted on Rat 7–3, left back side, is highlighted with a red star). In the rat group implanted for 21 days, 2 electrodes had lost the gold layer (Rat 21–2, left side and Rat

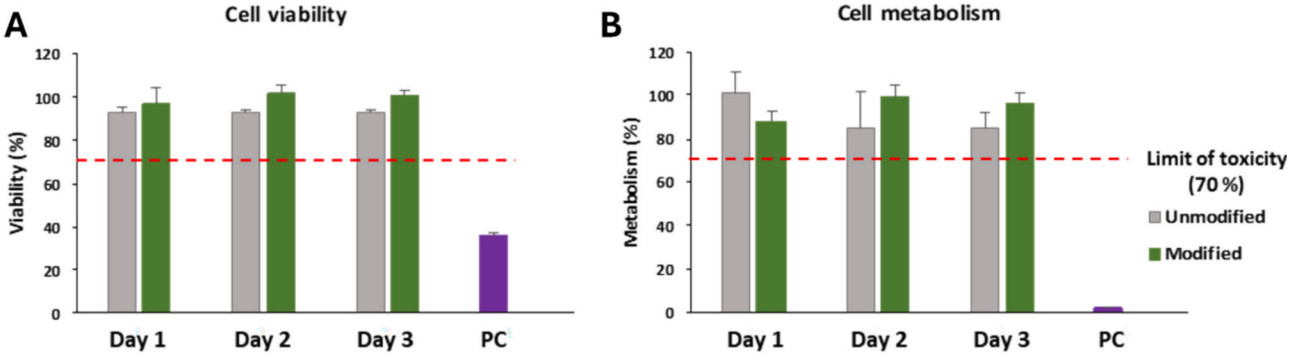

Fig. 8. Assessment of electrode cytotoxicity. (A) Cell survival and (B) cell metabolism were assessed by Neutral Red and MTT assays, with L929 cells incubated for 24 h in culture medium (providing the 100 %), or in the extracts obtained by incubation of electrodes, either unmodified (grey) or modified with the osmium-based polymer, GOx and PEDGE, for 24 h (green bars) during 3 successive days ("Day1", "Day2", and "Day3" extracts). "PC" is a positive control of toxicity obtained by adding 0.1 % Triton-X100 (*v*/v) in the culture medium. The red line defines the limit of toxicity (70 %). All the data are presented as mean ± s.d. ($n = 4$/group). (For interpretation of the references to colour in this figure legend, the reader is referred to the web version of this article.)

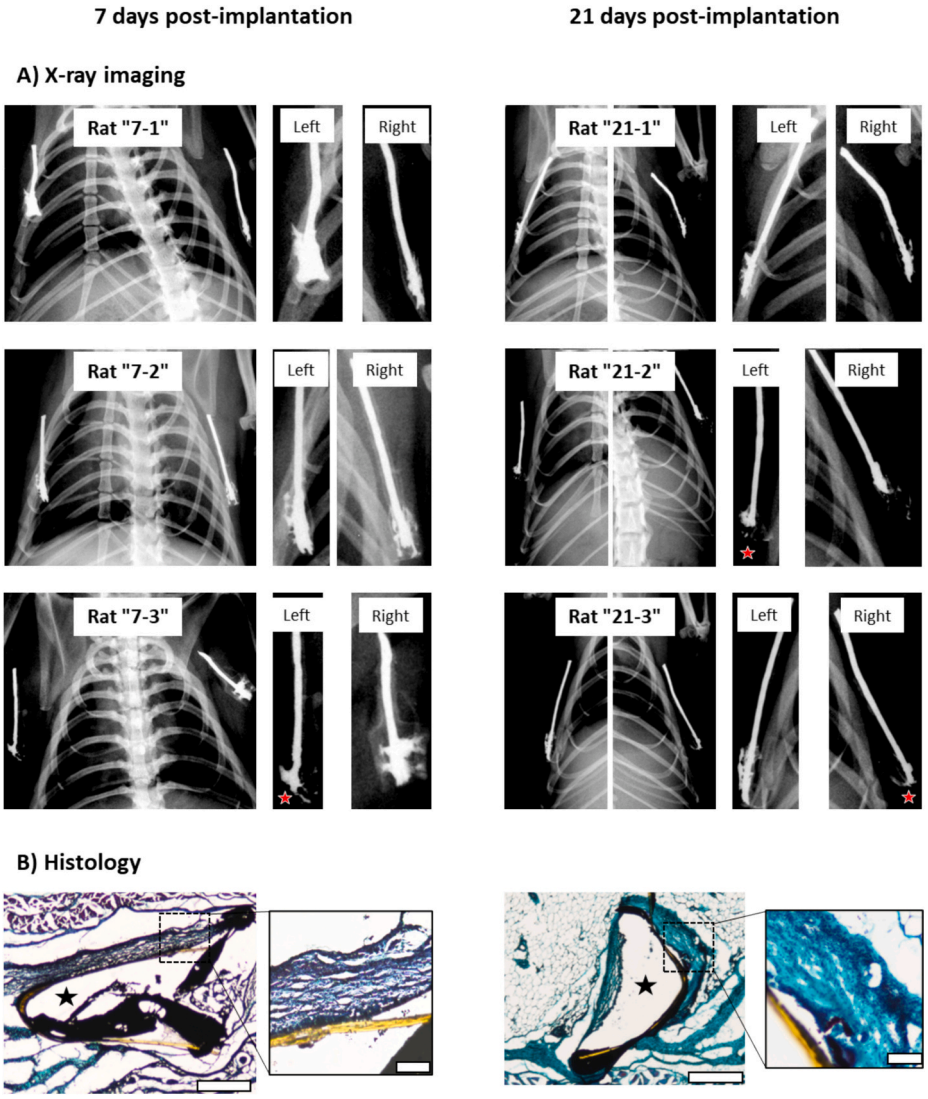

Fig. 9. Analysis of implanted electrodes after subcutaneous implantation in rats. (A) X-ray imaging of rats implanted with NPGs, after 7 days (left images) and 21 days (right images). Left and right refer to the magnified electrode images. Apparent loss of the gold layer is highlighted with a red star. (B) Representative sections stained by the Masson's Trichrome staining protocol. A black star shows the volume free of tissue. The left picture is from Rat 7–2, right electrode and the right picture from Rat 21–3, left side. Scale bars: 500 μm (100 μm in the magnified pictures). (For interpretation of the references to colour in this figure legend, the reader is referred to the web version of this article.)

21–3, right side, red stars). After dissection and Masson's Trichrome staining (that stains cell nuclei in purple and collagen fibres in blue-green), we observed that all the electrodes were bent after 7 days, inflammatory cells were detected in a cell layer surrounding the volume occupied by the electrode (Fig. 9 B, black star). After 21 days, inflammation was still detected, and a cellularized and vascularized capsule characterized by a loose collagen deposition surrounded the electrode and a large volume without regenerated tissue, suggesting that electrode mobility prevented the formation of granulation tissue. No difference in the tissue structure between the functionalised gold-MPC side and the dielectric paste side was evidenced.

4. Conclusions

Herein, we report the development of a glucose electrode on a Kapton® support for use as an implantable device. NPG electrodes were modified with GOx and a redox osmium complex-based hydrogel and then coated with a zwitterionic polymer (MPC). Low levels of cytotoxicity were confirmed by exposing fibroblasts to extracts of the uncoated modified electrodes (GOx/Os(bpy)$_2$Cl PVI/PEDGE) according to ISO10993-5. The electrochemical performance of GOx/Os(bpy)$_2$Cl PVI/PEDGE/MPC was evaluated in solutions of buffer and artificial plasma and displayed Michaelis and Menten behaviour with V_{MAX} of 211 ± 13 and 113 ± 10 μA cm^{-2}, K_{Mapp} of 6.1 ± 0.8 and 2.1 ± 0.4 mM and linear detection ranges of 1–4 and 1–2.5 mM, in buffer and artificial plasma, respectively. The ability of the electrode to withstand mechanical stress was evaluated in vitro and in vivo. The stress testing demonstrated that the electrode could withstand 160 deformations. On implantation of the electrodes in the subcutaneous tissue of a rat, the electrodes were stable for up to one week. Electrode movements resulting from muscular contractions at the implant sites likely prevented tissue regeneration due to electrodes not firmly fixed to the subcutaneous tissue. Inflammation of the tissue after 7 and 21 days was confirmed by histological analysis of the implant site suggesting that a more rigid support and optimised geometry may be required. The results demonstrate that the coated Kapton^{Ci}-based electrodes have the potential to operate in subcutaneous tissue for a period of at least one week. Improvements in the response of the sensor for operation in a complex environment may be achieved by further protecting the enzymes from potential inhibitors, variation of the NPG thickness layer and variation of redox polymer, enzyme and cross-linker ratios for better performances.

CRediT authorship contribution statement

Denise Demurtas: Writing – original draft, Methodology, Investigation, Formal analysis, Data curation. **Julia Alvarez-Malmagro:** Writing – review & editing, Investigation. **Arvind Rathore:** Investigation. **Tanushree Mandal:** Investigation. **Andrés Felipe Quintero-Jaime:** Formal analysis. **Serguei Belochapkine:** Investigation. **Anna Lielpetere:** Investigation. **Kavita Jayakumar:** Investigation. **Dónal Leech:** Resources, Investigation, Funding acquisition. **Wolfgang Schuhmann:** Resources, Project administration, Investigation, Funding acquisition, Conceptualization. **Nicolas Mano:** Resources, Methodology, Investigation, Funding acquisition. **Claudine Boiziau:** Resources, Methodology, Investigation, Funding acquisition, Formal analysis. **Edmond Magner:** Writing – review & editing, Supervision, Resources, Methodology, Investigation.

Declaration of competing interest

The authors declare that they have no known competing financial interests or personal relationships that could have appeared to influence the work reported in this paper.

Acknowledgements

This work has received funding from the European Union's Horizon 2020 research and innovation MSCA ITN program under grant agreement N°813006, IMPLANTSENS. The authors thank the animal house A1 facility at the University of Bordeaux (France) and Simon Bendl (UL) for designing the tool for mechanical stress application.

Appendix A. Supplementary data

Supplementary data to this article can be found online at https://doi.org/10.1016/j.bioelechem.2025.108949.

Data availability

Data will be made available on request.

References

[1] S.R. Heller, Self-monitoring of blood glucose: a promise still unfulfilled? Diabetologia 57 (2014) 847–849, https://doi.org/10.1007/s00125-014-3184-1.
[2] H. Teymourian, A. Barfidokht, J. Wang, Electrochemical glucose sensors in diabetes management: an updated review (2010−2020), Chem. Soc. Rev. 49 (2020) 7671–7709, https://doi.org/10.1039/d0cs00304b.
[3] G. Rocchitta, A. Spanu, S. Babudieri, G. Latte, G. Madeddu, G. Galleri, S. Nuvoli, P. Bagella, M.I. Demartis, V. Fiore, R. Manetti, P.A. Serra, Enzyme biosensors for biomedical applications: strategies for safeguarding analytical performances in biological fluids, Sensors (Basel) 16 (2016) 780, https://doi.org/10.3390/s16060780.
[4] S. Vaddiraju, D.J. Burgess, I. Tomazos, F.C. Jain, F. Papadimitrakopoulos, Technologies for Continuous Glucose Monitoring: current problems and future promises, J. Diabetes Sci. Technol. 4 (2010) 1540–1562, https://doi.org/10.1177/193229681000400632.
[5] L. Heinemann, Finger pricking and pain: a never ending story, J. Diabetes Sci. Technol. 2 (2008) 919–921, https://doi.org/10.1177/193229680800200526.
[6] S. Emaminejad, W. Gao, E. Wu, Z.A. Davies, H. Yin Yin Nyein, S. Challa, S.P. Ryan, H.M. Fahad, K. Chen, Z. Shahpar, S. Talebi, C. Milla, A. Javey, R.W. Davis, Autonomous sweat extraction and analysis applied to cystic fibrosis and glucose monitoring using a fully integrated wearable platform, Proc. Natl. Acad. Sci. 114 (2017) 4625–4630, https://doi.org/10.1073/pnas.1701740114.
[7] J. Wu, H. Liu, W. Chen, B. Ma, H. Ju, Device integration of electrochemical biosensors, nature reviews, Bioengineering 1 (2023) 346–360, https://doi.org/10.1038/s44222-023-00032-w.
[8] C. Sun, Z. Cheng, J. Abu-Halimah, B. Tian, Perspectives on tissue-like bioelectronics for neural modulation, iScience 26 (2023) 106715, https://doi.org/10.1016/j.isci.2023.106715.
[9] Y. Zhao, B. Wang, J. Tan, H. Yin, R. Huang, J. Zhu, S. Lin, Y. Zhou, D. Jelinek, Z. Sun, K. Youssef, L. Voisin, A. Horrillo, K. Zhang, B.M. Wu, H.A. Coller, D.C. Lu, Q. Pei, S. Emaminejad, Soft strain-insensitive bioelectronics featuring brittle materials, Science 378 (2022) 1222–1227, https://doi.org/10.1126/science.abn5142.
[10] M. Devi, M. Vomero, E. Fuhrer, E. Castagnola, C. Gueli, S. Nimbalkar, M. Hirabayashi, S. Kassegne, T. Stieglitz, S. Sharma, Carbon-based neural electrodes: promises and challenges, J. Neural Eng. 18 (2021) 041007, https://doi.org/10.1088/1741-2552/ac1e45.
[11] X. Xiao, T. Siepenkoetter, P.O. Conghaile, D. Leech, E. Magner, Nanoporous gold-based biofuel cells on contact lenses, ACS Appl. Mater. Interfaces 10 (2018) 7107–7116, https://doi.org/10.1021/acsami.7b18708.
[12] A. Zebda, C. Gondran, A. Le Goff, M. Holzinger, P. Cinquin, S. Cosnier, Mediatorless high-power glucose biofuel cells based on compressed carbon nanotube-enzyme electrodes, Nat. Commun. 2 (2011) 370, https://doi.org/10.1038/ncomms1365.
[13] P. Cinquin, C. Gondran, F. Giroud, S. Mazabrard, A. Pellissier, F. Boucher, J. P. Alcaraz, K. Gorgy, F. Lenouvel, S. Mathe, P. Porcu, S. Cosnier, A glucose biofuel cell implanted in rats, PLoS One 5 (2010) e10476, https://doi.org/10.1371/journal.pone.0010476.
[14] D. Saha, C.L. Heldt, M.F. Gencoglu, K.S. Vijayaragavan, J. Chen, A. Saksule, A study on the cytotoxicity of carbon-based materials, Mater. Sci. Eng. C Mater. Biol. Appl. 68 (2016) 101–108, https://doi.org/10.1016/j.msec.2016.05.094.
[15] A. Heller, B. Feldman, Electrochemical glucose sensors and their applications in diabetes management, Chem. Rev. 108 (2008) 2482–2505, https://doi.org/10.1021/cr068069y.
[16] Q. Huang, J. Chen, Y. Zhao, J. Huang, H. Liu, Advancements in electrochemical glucose sensors, Talanta 281 (2025) 126897, https://doi.org/10.1016/j.talanta.2024.126897.
[17] R. Bennett, E. Blochouse, D. Leech, Effect of individual plasma components on the performance of a glucose enzyme electrode based on redox polymer mediation of a flavin adenine dinucleotide-dependent glucose dehydrogenase, Electrochim. Acta 302 (2019) 270–276, https://doi.org/10.1016/j.electacta.2019.02.039.

[18] S. Capuani, G. Malgir, C.Y.X. Chua, A. Grattoni, Advanced strategies to thwart foreign body response to implantable devices, Bioeng. Transl. Med. 7 (2022) e10300, https://doi.org/10.1002/btm2.10300.
[19] P. Singh, J. Ram, V. Chauhan, P.M.G. Nambissan, S.K. Gupta, S. Kumar, S. K. Sharma, P.D. Sahare, R. Kumar, High dose gamma radiation exposure upon Kapton-H polymer for modifications of optical, free volume, structural and chemical properties, Optik 205 (2020) 164244, https://doi.org/10.1016/j.ijleo.2020.164244.
[20] C.P. Constantin, M. Aflori, R.F. Damian, R.D. Rusu, Biocompatibility of polyimides: a Mini-review, Mater. (Basel) 12 (2019) 3166, https://doi.org/10.3390/ma12193166.
[21] J. Anderson, S. Cramer, Perspectives on the inflammatory, healing, and foreign body responses to biomaterials and medical devices, in: S.F. Badylak (Ed.), Host Response to Biomaterials, Academic Press, Oxford, 2015, pp. 13–36.
[22] A. Muhs, T. Bobrowski, A. Lielpetere, W. Schuhmann, Catalytic biosensors operating under quasi-equilibrium conditions for mitigating the changes in substrate diffusion, Angew. Chem. Int. Ed. Eng. 61 (2022) e202211559, https://doi.org/10.1002/anie.202211559.
[23] N.G. Welch, D.A. Winkler, H. Thissen, Antifibrotic strategies for medical devices, Adv. Drug Deliv. Rev. 167 (2020) 109–120, https://doi.org/10.1016/j.addr.2020.06.008.
[24] V. Yesilyurt, O. Veiseh, J.C. Doloff, J. Li, S. Bose, X. Xie, A.R. Bader, M. Chen, M. J. Webber, A.J. Vegas, R. Langer, D.G. Anderson, A facile and versatile method to endow biomaterial devices with Zwitterionic surface coatings, Adv. Healthc. Mater. 6 (2017), https://doi.org/10.1002/adhm.201601091.
[25] L. Zhang, Z. Cao, T. Bai, L. Carr, J.R. Ella-Menye, C. Irvin, B.D. Ratner, S. Jiang, Zwitterionic hydrogels implanted in mice resist the foreign-body reaction, Nat. Biotechnol. 31 (2013) 553–556, https://doi.org/10.1038/nbt.2580.
[26] Z. Zhang, J. Borenstein, L. Guiney, R. Miller, S. Sukavaneshvar, C. Loose, Polybetaine modification of PDMS microfluidic devices to resist thrombus formation in whole blood, Lab Chip 13 (2013) 1963–1968, https://doi.org/10.1039/c3lc50302j.
[27] C. Mercer, R. Bennett, P.O. Conghaile, J.F. Rusling, D. Leech, Glucose biosensor based on open-source wireless microfluidic potentiostat, Sensors Actuators B Chem. 290 (2019) 616–624, https://doi.org/10.1016/j.snb.2019.02.031.
[28] A. Lielpetere, K. Jayakumar, D. Leech, W. Schuhmann, Cross-linkable polymer-based multi-layers for protecting electrochemical glucose biosensors against uric acid, ascorbic acid, and biofouling interferences, ACS Sens. 8 (2023) 1756–1765, https://doi.org/10.1021/acssensors.3c00050.
[29] J.D. Yeager, D.F. Bahr, Microstructural characterization of thin gold films on a polyimide substrate, Thin Solid Films 518 (2010) 5896–5900, https://doi.org/10.1016/j.tsf.2010.05.070.
[30] S. Trasatti, O. Petrii, Real surface area measurements in electrochemistry, Pure Appl. Chem. 63 (1991) 711–734, https://doi.org/10.1351/pac199163050711.
[31] T. Siepenkoetter, U. Salaj-Kosla, X. Xiao, P.O. Conghaile, M. Pita, R. Ludwig, E. Magner, Immobilization of redox enzymes on Nanoporous gold electrodes: applications in biofuel cells, Chempluschem 82 (2017) 553–560, https://doi.org/10.1002/cplu.201600455.
[32] C.A. Burtis, E.R. Ashwood, J.E. Aldrich, N.W. Tietz, Tietz fundamentals Clini. Chem. No Title (1996).
[33] M.D. Scanlon, U. Salaj-Kosla, S. Belochapkine, D. MacAodha, D. Leech, Y. Ding, E. Magner, Characterization of nanoporous gold electrodes for bioelectrochemical applications, Langmuir 28 (2012) 2251–2261, https://doi.org/10.1021/la202945s.
[34] K.R. Sindhu, N. Bansode, M. Remy, C. Morel, R. Bareille, M. Hagedorn, B. Hinz, P. Barthelemy, O. Chassande, C. Boiziau, New injectable self-assembled hydrogels that promote angiogenesis through a bioactive degradation product, Acta Biomater. 115 (2020) 197–209, https://doi.org/10.1016/j.actbio.2020.08.012.
[35] T. Siepenkoetter, U. Salaj-Kosla, X. Xiao, S. Belochapkine, E. Magner, Nanoporous gold electrodes with Tuneable pore sizes for bioelectrochemical applications, Electroanalysis 28 (2016) 2415–2423, https://doi.org/10.1002/elan.201600249.
[36] Y.S. Sun, T.J. Balk, Mechanical behavior and microstructure of nanoporous gold films, MRS Online Proceed. Library (OPL) 924 (2006).
[37] N.J. Briot, T.J. Balk, Focused ion beam characterization of deformation resulting from nanoindentation of nanoporous gold, MRS Commun. 8 (2018) 132.
[38] P.A. Jenkins, S. Boland, P. Kavanagh, D. Leech, Evaluation of performance and stability of biocatalytic redox films constructed with different copper oxygenases and osmium-based redox polymers, Bioelectrochemistry 76 (2009) 162–168, https://doi.org/10.1016/j.bioelechem.2009.04.008.
[39] S. Shachneva, A. Lielpetere, W. Schuhmann, Pencil-Lead-Based Quasi-Equilibrium Glucose Biosensors, Adv. Sensor Res. 3 (2024) 2400024, https://doi.org/10.1002/adsr.202400024.
[40] E. Maestri, The 3Rs principle in animal experimentation: a legal review of the state of the art in Europe and the case in Italy, Bio.Tech. (Basel) 10 (2021) 9, https://doi.org/10.3390/biotech10020009.
[41] U. Salaj-Kosla, M.D. Scanlon, T. Baumeister, K. Zahma, R. Ludwig, P.O. Conghaile, D. MacAodha, D. Leech, E. Magner, Mediated electron transfer of cellobiose dehydrogenase and glucose oxidase at osmium polymer-modified nanoporous gold electrodes, Anal. Bioanal. Chem. 405 (2013) 3823–3830, https://doi.org/10.1007/s00216-012-6657-4.